analytical chemistry

Article

pubs.acs.org/ac

Capping Agent-Free Gold Nanostars Show Greatly Increased Versatility and Sensitivity for Biosensing

Debrina Jana, Carlos Matti, Jie He, and Laura Sagle*

Department of Chemistry, College of Arts and Sciences, University of Cincinnati, 301 West Clifton Court, Cincinnati Ohio 45221-0172, United States

Supporting Information

ABSTRACT: We report the first assessment of the plasmonic biosensing capabilities of capping agent-free gold nanostars. Capping agent removal was carried out using aqueous solutions of sodium borohydride, which yielded a refractive index sensitivity of 474 nm/RIU for the polyvinylpyrrolidone (PVP)-free nanostars compared with 98 nm/RIU for PVP-coated gold nanostars. Following PVP removal, biotinylated thiol and streptavidin protein were added to the nanostars, which resulted in red shifts as large as 51 nm and a limit of detection as low as 0.1 pM. Refractive index-based sensing of prostate specific antigen (PSA) both in buffer and serum was then carried out and was shown to yield shifts as large as 127 nm and have a limit of detection of 100 pM in serum. Last, a sandwich assay involving PSA was developed to aggregate the nanostars together for greater sensitivity. The sandwich assay did, indeed, give shifts close to 200 nm and was capable of detecting 10^{-17} M PSA in serum. The greatly increased sensitivity and amenability to functionalization of PVP-free gold nanostars should prove useful in applications ranging from catalysis to drug delivery.

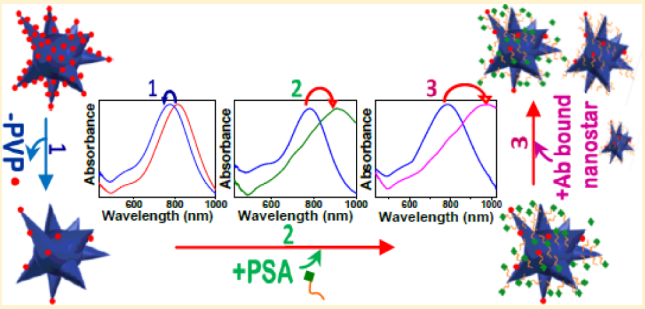

Plasmonic gold nanostructures, both in solution and on surfaces, have been shown to be extremely useful in applications such as optics and photonics,[1,2] electronics,[3] catalysis,[4] drug delivery,[5] and biosensing.[6] Their properties arise from collective oscillations of electrons in the conduction band upon irradiation, referred to as the localized surface plasmon resonance (LSPR).[7] The LSPR frequency is dependent on the size and shape of the nanoparticle as well as the local environment.[8] Biological applications are particularly attractive with gold nanoparticles because their toxicity is less than that of silver.[9] In addition, the plasmonic properties and electromagnetic field enhancements can be tailored by changing the shape of the nanoparticle. For example, spherical gold colloids absorb mainly visible light, whereas anisotropic gold structures with pointy edges or hollow interiors absorb in the infrared region of the spectrum.[10] For most in vivo biological applications, plasmon absorptions in the infrared (offering high penetration depth) and increased sensitivity to the local environment is optimal.[11,12] Recently, a renaissance of complex, anisotropic gold nanostructures, such as nanocubes,[13,14] nanorods,[15] nanoflowers,[16] nanobipyrimids,[17] and nanostars,[18] have been shown to have optimal resonance wavelength (for sizes <130 nm), limited toxicity, good aqueous solubility, and greatly increased refractive index sensitivity. These structures have already been valuable tools in applications such as drug delivery,[19] cellular imaging,[20] and biosensing.[21]

Gold nanostars, first synthesized in 2006, have been particularly attractive for surface-enhanced Raman spectroscopy (SERS) and LSPR biosensing applications because their protruding tips have high electromagnetic field enhancements.[22,23] Indeed, SERS measurements have been achieved with single gold nanostars, which is only possible with aggregates of spherical gold colloids.[24] Another recent study investigated the LSPR biosensing of gold nanostars coupled to a planar gold film and shows remarkable zeptomole sensitivity.[25] In addition, gold nanostars were able to achieve attomole detection of prostate-specific antigen (PSA) in serum through the growth of a silver shell that was dependent on PSA concentration.[26] Although this study yields exquisite sensitivity to PSA, detection of another protein of interest would require secondary antibody binding and the chemical linkage of this antibody to glucose oxidase.

Traditional refractive-index-based biosensing utilizing gold nanostars, which is the most versatile, remains limited because the shifts in plasmon resonance from a bulk solution of gold nanostars, upon addition of protein, is quite small. A recent study has evaluated the LSPR shifts upon addition of a biotinylated bovine serum albumin (BSA), followed by streptavidin, to individual gold nanostars using dark-field microscopy.[27] Unfortunately, the largest shift observed upon addition of saturating concentrations of protein was only 9 nm. One likely explanation for this lack of sensitivity of gold nanostars in refractive-index-based LSPR biosensing is that the

Received: January 3, 2015
Accepted: February 27, 2015
Published: February 27, 2015

DOI: 10.1021/acs.analchem.5b00014
Anal. Chem. 2015, 87, 3964−3972

surface itself is not accessible, and the accessible sites are farther removed from the surface of the nanostars. Because the gold nanostars are synthesized using polyvinylpyrrolidone (PVP) as a capping agent, it is feasible that PVP is preventing the binding of molecules of interest directly to the nanostar surface, thus limiting shifts in the LSPR frequency upon protein binding (see Figure 1).

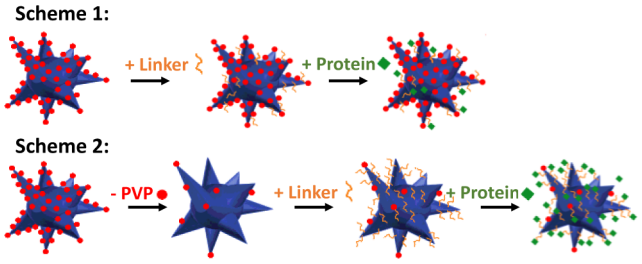

Figure 1. Traditional LSPR biosensing with PVP-capped gold nanostars, Scheme 1. LSPR biosensing in which the PVP is removed before the linker is added, Scheme 2. It is expected that PVP removal will allow for greater linker and protein binding, increasing biosensing capabilities.

Herein, we have removed the capping agent, PVP, from gold nanostars and evaluated the LSPR biosensing potential. This removal of PVP is expected to increase functionality and biosensing capabilities of the gold nanostars. The PVP was removed from the surface of the nanostars using sodium borohydride, which was recently reported to remove PVP from gold colloids.[28] A large blue shift is observed in the bulk UV−vis spectrum of the gold nanostars, confirming PVP removal. After removal of the PVP, biosensing measurements were carried out with streptavidin and PSA proteins through a biotin−polyethylene glycol (PEG)−thiol (MW = 5000 g/mol) linker or carbodiimde (EDC) coupling of a PSA antibody to a mercaptoundecanoic acid (MUA)/octanethiol (OT) linker. Interestingly, shifts as large as 51 and 127 nm are observed upon addition of biotin/streptavidin and antibody/PSA respectively. As suggested by the large shifts commensurate with protein binding, the refractive index sensitivity was measured to be roughly 4−5 times that of gold colloids and twice that of gold nanorods.[29] In addition, the surface enhanced Raman spectroscopy (SERS) signal of capping agent-free gold nanostars was investigated through the addition of Malachite Green isothiocyanate (MGIT), and the SERS signal was roughly 100 times greater than nanostars containing PVP. Next, PSA binding to PVP-free gold nanostars was further evaluated in mouse serum, and the dissociation constant, K_d, is estimated at 1×10^{-9} M with a limit of detection of 1×10^{-10} M. Last, a sandwich assay is developed in which nanostars coated in PSA antibody are aggregated via the PSA protein. This aggregation assay produced much larger shifts in the plasmon resonance (~200 nm) and showed a very low limit of detection of 1×10^{-17} M PSA in mouse serum samples. Thus, gold nanostars without PVP offer great potential as sensitive biosensors capable of both in vitro and in vivo applications.

EXPERIMENTAL SECTION

Synthesis of Gold Nanostars. Prior to synthesis, all glassware was cleaned using aqua regia (3:1 volume ratio of 37% hydrochloric acid and concentrated nitric acid). Synthesis of gold nanostars was carried out following the method reported by the Liz-Marzán group with slight modifications.[18] Briefly, in the first step, small gold colloids of 16 nm in diameter were synthesized according to the standard sodium citrate reduction method.[30,31] In the second step, these gold colloids were functionalized by PVP by mixing the colloidal solution with PVP (MW = 10 000) (Sigma-Aldrich) under stirring for 24 h at room temperature.[32] PVP-functionalized nanoparticles were then transferred to ethanol, through centrifugation, removal of supernatant, and addition of ethanol. In the final step, 82 μL of aqueous 50 mM $HAuCl_4$ (Sigma-Aldrich) solution was mixed with 15 mL of 10 mM PVP (MW = 29 000) (Sigma-Aldrich) solution in *N*,*N*-dimethylformamide (Sigma-Aldrich), followed by the rapid addition of 16 nm gold seeds (43 μL) prepared in the second step. A color change of the solution from pink to colorless and finally to blue within 15 min indicated the formation of gold nanostars in the solution. The nanostar solution was centrifuged, the supernatant was discarded, and the gold nanostars were transferred to ethanol or water for further measurements.

Removal of PVP From Gold Nanostars. Desorption of PVP from gold nanostars was carried out by treating the nanostar solution with an aqueous $NaBH_4$ (Fluka) solution. Typically, 100−200 μL of 0.05 M freshly prepared $NaBH_4$ solution (in water) was added to 1 mL of 0.0158 M nanostar solution (in ethanol) with vigorous stirring and occasional sonication. After every 15 min, the solution was centrifuged for 5 min at 14 000 rpm (Sorvall Legent XTR, Thermo Scientific), the supernatant was discarded, and the pellet was dispersed in ethanol by sonication (FS60D, Thermo Scientific) and replenished by the same volume of aqueous 0.05 M $NaBH_4$ solution. This whole process was repeated for up to 60 min. To directly compare PVP-free nanostars with various biological molecules bound, UV−vis measurements of all samples were taken in doubly distilled water.

Addition of Biotin and Streptavidin. Before the addition of biotin or streptavidin, the remaining hydride on the 0.0158 M solution of PVP-free nanostars was washed several times with doubly distilled water through centrifugation (14 000 rpm for 5 min) and resuspended in solution. For the biosensing experiments, first 1 mL of 1.28 mM of biotin−PEG−thiol (MW = 5000 g/mol) (Nanocs, Inc.) was added to the above 60-min-BH_4^--treated nanostar sample under vigorous stirring for 24 h. Next, the solution was centrifuged, the supernatant was removed, and fresh water was added. This washing of the excess biotin ligand was repeated three to four times, followed by centrifugation and addition of an aqueous solution of 1 μM streptavidin protein (Abcam, Inc.) in 50 mM HEPES (Fluka) buffer at pH 7. The nanostar−protein solution was gently shaken at 4 °C overnight and centrifuged the next day, and the supernatant was discarded and replaced with doubly distilled water for measurements. For the nonspecific binding measurements (control experiment shown in red in Supporting Information Figure S2), the same concentration, 0.0158 M, of PVP-free nanostars (containing no biotin ligand) was soaked overnight in different concentrations of streptavidin at 4 °C. The next day, the samples were centrifuged, and the supernatant was discarded and replaced with doubly distilled water for measurements.

Addition of Antibody and PSA. To functionalize the gold nanostars with PSA antibody, a self-assembled monolayer of 11-mercaptoundecanoic acid (MUA) and 1-octanethiol (OT) (Sigma-Aldrich) was first formed. A 1 mL solution of a mixture of MUA and OT in a 1:3 ratio was added to the above 60-min-

DOI: 10.1021/acs.analchem.5b00014
Anal. Chem. 2015, 87, 3964−3972

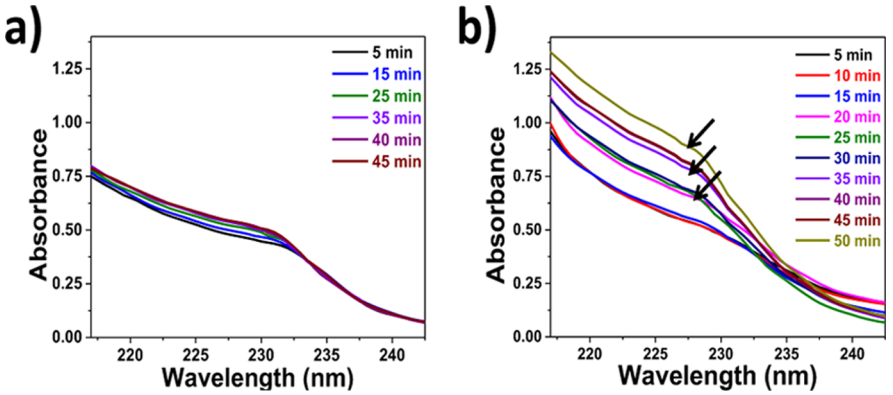

Figure 2. Removal of PVP from gold nanostars and its release into solution, as evidenced by the UV−vis absorption band at ∼230 nm. Spectra are taken every 5 min after the addition of one treatment of sodium borohydride, shown in part a. Spectra are taken every 5 min after repeated borohydride treatments every 15 min, indicated by black arrows in part b.

BH_4^--treated 0.0158 M nanostar sample under vigorous stirring overnight. Next, the nanostars were incubated in 1 mL of 5 mM aqueous *N*-hydroxysuccinimide, NHS (Thermo Scientific, Inc.), solution for 30 min, followed by centrifugation. This "activates" the COOH groups on the MUA to prepare for the coupling of the antibodies. The precipitated nanostars were then redispersed in 1 mL of 5 mM 1-ethyl-3-(3-(dimethylamino)propyl) carbodiimide HCl, EDC (Thermo Scientific, Inc.), in HEPES buffer (pH 7) and 10 μL of 10^{-9} M of rabbit monoclonal antibody (specific to human PSA) (Abcam, Inc.). This mixture was kept at 4 °C with gentle shaking for 1−2 h. The antibody-coated nanostars were then centrifuged, the supernatant was discarded, and 500 μL of mouse serum was added. After 1 h, the solution was centrifuged; the supernatant was discarded; and the desired concentration of prostate specific antigen (ranging from 10^{-6} to 10^{-12} M), diluted in serum, was added; and the resulting solution was kept at 4 °C overnight. The next day, measurements were carried out by centrifuging and replacing the supernatant with doubly distilled water for UV−vis measurements. For nonspecific binding measurements (shown in red in Supporting Information Figure S4), MUA/OT-coated nanostars (without antibody) were soaked in various concentrations of PSA in serum overnight at 4 °C, followed by centrifugation and redissolving in doubly distilled water for measurements.

PSA Detection Using Nanostar Agglomeration. To detect very low concentrations of PSA (10^{-14}−10^{-20} M), PSA was sandwiched between two batches of antibody-coated nanostars. For this, mouse monoclonal antibody (Abcam, Inc.) was first conjugated to one batch of MUA/OT-coated nanostars using NHS and EDC as described above. Next, this solution was added to the other batch of nanostars, which has been conjugated with rabbit polyclonal antibody (Abcam, Inc.) specific for a different region of the PSA protein using EDC and NHS as described above. The desired concentration of PSA was then added to a 50:50 mixture of the two antibody-coated nanostars and incubated overnight in either HEPES buffer or 100% mouse serum (Sigma-Aldrich, Inc.). The next day, the mixture was centrifuged and used for measurements after replacing the supernatant with doubly distilled water. Nonspecific binding measurements were carried out by mixing the MUA/OT coated-nanostars with different concentrations of PSA overnight at 4 °C overnight, followed by centrifugation and replacing the supernatant with doubly distilled water.

LSPR Measurements. All measurements of the localized surface plasmon resonances were carried out using a USB2000+ vis−NIR (Ocean Optics, Inc.) configured with fiber optic cables and a cuvette holder. The data were collected using the SpectraSuite software provided by Ocean Optics, and each spectrum was constructed by averaging 100 scans, each collected with 4 ms integration time. Frequency values for the individual plasmon resonances were obtained by fitting the peaks of interest to a Gaussian function using Origin 9.0 software (OriginLab, Inc.).

SERS Experiments. Surface enhanced Raman spectroscopy was carried out by adding 100 μL of 10^{-4} M MGIT (Life Technologies, Inc.) in ethanol to a 60-min-BH_4^--treated nanostar sample under vigorous stirring overnight. Excess dye was discarded by centrifugation, and the pellet was dispersed in doubly distilled water by sonication. A drop of the dispersion was transferred into a small borosilicate glass capillary tube (Kimble Chase) having a 1 mm inner diameter. It was placed on the stage of a Renishaw inVia Raman microscope equipped with a Renishaw MS20 nanopositioning stage. The laser intensity at the samples was 1.07 mW from a 633 nm helium−neon laser. The exposure time for all measurements was 10 s, and each spectrum was constructed from 1 scan with a grating of 1200 mm^{-1}. Between different Raman sessions, the 520.7 cm^{-1} peak of a silicon wafer was used to calibrate the spectrograph. Raman spectra of 100 nm gold colloids (Ted Pella, Inc.) and a gold nanostar sample that was not treated with BH_4^- (referred to as with PVP) having similar concentration was used for comparison. The concentrations of all colloidal suspensions (in particles/milliliter) were measured using dynamic light scattering from the Nanotrac Analyzer System (Microtrac, Inc.). It was also ensured that the same concentration of dye solution was added to colloidal suspensions of the same concentration.

TEM Measurements. Transmission electron microscopy (TEM) studies were carried out using an FEI Phillips CM-20 at 200 eV. Samples were prepared on ultrathin carbon type-A, 400 mesh Cu grids coated with Formvar (Ted Pella). Samples were first diluted in 50 mM HEPES buffer and then micropipetted dropwise onto the grid surface. Excess nanoparticle solution was subsequently wicked away.

RESULTS AND DISCUSSION

PVP Removal. PVP removal was accomplished through the addition of sodium borohydride to a solution of gold nanostars

DOI: 10.1021/acs.analchem.5b00014
Anal. Chem. 2015, 87, 3964−3972

containing PVP. It has been suggested that the mechanism of PVP removal with sodium borohydride involves replacement of PVP by the hydride ion itself, which has a stronger affinity for gold.[28] The hydride ion can be subsequently removed through reaction with H_3O^+ to form H_2 gas in solution, which is accomplished by washing with copious amounts of water or the addition of small amounts of acid (see Experimental Section). This PVP removal from the nanostars was first monitored through the free PVP released into the solution, which absorbs ~230 nm in the UV−vis spectrum.[33,34]

Figure 2a shows the absorption spectra of PVP in solution every 5 min after the addition of one batch of 0.05 M sodium borohydride. Indeed, the absorption band due to PVP increases slightly over the course of 45 min; however, the later time points at 40 and 45 min show overlapping spectra, indicating no further extraction of PVP. This is substantiated by recent studies that show that borohydride reacts with H_3O^+ in aqueous solution over time to form H_2 gas, reducing the amount of hydride ion available for PVP removal.[35,36] To more effectively remove PVP from the gold nanostars, after the addition of one batch of borohydride, the solution was subjected to centrifugation to pellet the nanostars, and another fresh batch of borohydride was added. This process was repeated every 15 min, and the UV−vis spectrum of the supernatant was measured every 5 min. As shown in Figure 2b, replenishing at 15 min intervals with fresh borohydride during a 45 min period yielded a significant increase in the amount of PVP extracted from the nanostars. After the third borohydride treatment, at 45 min, it was noted that less of a change in PVP concentration was observed, indicating that desorption of PVP from the gold nanostars had slowed significantly. Thus, replenishing every 15 min with borohydride for approximately 50−60 min appears to be most effective for removing PVP from the gold nanostars.

In addition to directly measuring the PVP released into solution from the nanostars, the LSPR spectrum of the nanostars themselves was measured as they were subjected to sodium borohydride. The LSPR spectrum of gold nanostars in solution has been characterized by previous reports and consists of multiple peaks, with the main absorption in the near-infrared.[18,22] PVP removal was expected to yield blue shifts in the LSPR spectrum of the nanostars as a result of a decrease in the refractive index of the aqueous solution (refractive index of 1.33) versus PVP (refractive index of ~1.42) at the nanoparticle surface. Indeed, large blue shifts of 45 nm were observed for the broad high wavelength peak associated with the gold nanostars (see Figure 3a). The time scale for PVP removal for the high wavelength peak of the gold nanostars is much faster than that shown for PVP being released into solution (see Figure 2). The most drastic shift occurs within the first 15 min, before the first borohydride replenishing, whereas the treatments after 15 min show only a modest shift of 12 nm. This inconsistency in the UV−vis data shown in Figures 2 and 3 could be explained by the fact that the nanostar LSPR spectrum is most likely dominated by the tips of the nanostars, whereas the PVP release in solution would encompass both the tips and the core of the nanostars. Recent experimental and theoretical work carried out on single gold nanostars shows that the plasmon resonances observed are, in fact, dominated by the tips of the stars and are polarization-dependent.[37] Indeed, these tips of the nanostar are expected to have the largest field enhancement and show the most pronounced shift upon a change in environment.[38,39] This

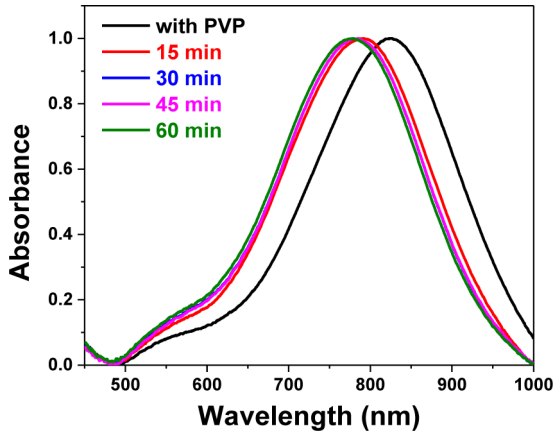

Figure 3. A dramatic blue shift of 45 nm is observed in the LSPR spectrum of the gold nanostars upon PVP removal.

notion is supported by a recent study in which the tips of the nanostars were intentionally rounded by changing the seed concentration, and a systematic blue shift from ~850 to ~700 nm was observed.[40]

On the basis of these studies, the main peak observed here is most likely due to the longitudinal plasmon mode of the nanostar tips, which would be expected to be more accessible to solvent. Interestingly, the continued release of PVP into the solution over longer time scales, observed in Figure 2, is most likely due to PVP removal from the core region, which would be less labile and possibly less accessible to the solvent. This difference in time scales for PVP removal has interesting implications for drug delivery applications, in which it is often desirable to have a burst of drug released quickly while the rest is followed by a slower, more linear release over time.

The fast time scales of PVP removal from the nanostar tips is further substantiated by SERS data. In these studies, the nanostar solution was first treated with sodium borohydride, pelleted, and then dissolved in a MGIT solution, which serves as a Raman reporter molecule. It was expected that as more PVP was removed, more MGIT would bind, increasing the SERS signal observed. As shown in Figure 4, the SERS signal

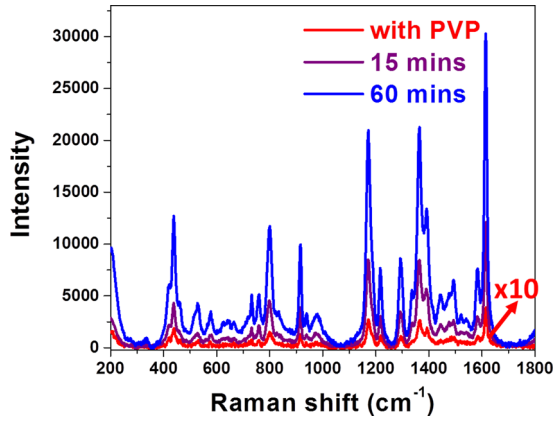

Figure 4. SERS of gold nanostars containing MGIT as a reporter molecule. Gold nanostars with PVP (red), nanostars after one 15 min sodium borohydride treatment (purple), and nanostars after four consecutive 15 min sodium borohydride treatments (blue). A 100-fold SERS enhancement is observed when comparing samples containing PVP with those treated with borohydride for 60 min.

DOI: 10.1021/acs.analchem.5b00014
Anal. Chem. 2015, 87, 3964−3972

for MGIT is, indeed, much larger for borohydride-treated nanostars. Upon replenishing with 0.05 M sodium borohydride four times, every 15 min, for a total of 60 min, the SERS signal increased 100-fold over that of nanostars containing PVP. This 100-fold improvement in SERS intensity is considerably larger than that observed from repeatedly washing the PVP from gold nanostars, which yielded only a 15-fold SERS enhancement.[41] Even after only one 15 min borohydride treatment, the SERS intensity of the ~1600 cm^{-1} peak is within a factor of 2 of the sample treated for an hour. Because it is established that the SERS "hot spots" are located at the tips of the nanostars,[42] it is conceivable that most of the SERS enhancement is due to MGIT's binding to these tips. Thus, once again, PVP removal from the tips of the nanostars appears to happen quite rapidly, primarily within the first 15 min, and as shown in the next section, it is expected that the nanostar tips are also the most sensitive for LSPR biosensing.

The substantial blue shifts that accompany PVP removal in the plasmon resonances of the nanostars could also be explained by annealing of the nanostar tips upon borohydride treatment. To investigate this possibility, transmission electron microscopy (TEM) measurements were carried out on samples both before borohydride treatment and after a 1 h treatment (with replenishing every 15 min). As shown in Figure 5, the overall features of the nanostars, particularly the sharp tips, remain the same after a 1 h borohydride treatment. Thus, the blue shifts observed upon borohydride treatment of the nanostars are most likely due to PVP removal and not annealing. Additional evidence to support the association of blue shifts in the plasmon absorptions with PVP removal is provided in Figure S1 of the Supporting Information. Upon addition of PVP to the borohydride-treated nanostars, a red shift is observed yielding a full recovery of the original LSPR spectrum.

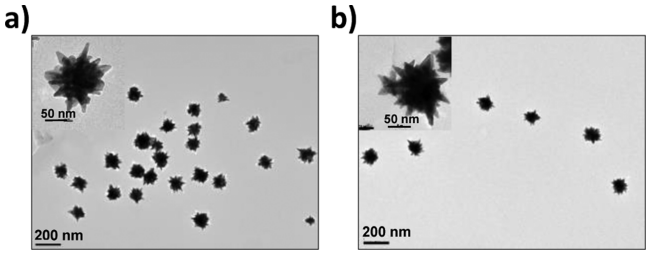

Figure 5. TEM of gold nanostars before sodium borohydride treatment (a) and after four 15 min sodium borohydride treatments (total of 60 min) (b).

Biosensing. To assess the biosensing capabilities of the PVP-free gold nanostars, the shifts in LSPR frequency that accompany the nanostars dissolved in solvents of different refraction indexes were measured. As shown in Figure 6, the refractive index sensitivity, or *m* values, for the plasmon resonances of the gold nanostars are calculated from a plot of LSPR shifts versus refractive index. As expected, the peak associated with the PVP-free nanostars show the highest *m* value of 474 nm/RIU, whereas the PVP-coated nanostars yield an *m* value of 98 nm/RIU. Thus, there is a large increase in refractive index sensitivity upon PVP-removal, yielding *m* values 4−5 times higher than the PVP-coated counterpart. This *m* value of the PVP-free nanostars is roughly twice reported for gold nanorods in solution and slightly larger than nanobipyrimids,[43] although it is important to note that both *m* values for nanorods and nanobipyrimids were obtained with capping agents present, which prevents large-scale protein binding needed to assess biosensing capabilities. Even though more sensitive nanostructures have been made (such as hollow nanocubes), to the best of our knowledge, the PVP-free gold nanostars represent the most sensitive, solution-phase, gold nanostructure capable of being functionalized to bind a protein of interest.

The large *m* values are evidenced by sizable shifts observed upon addition of a biotin−PEG−thiol linker, followed by varying concentrations of streptavidin protein. These shifts are shown in Supporting Information Figure S2 and tabulated, with standard deviations from at least three different samples, in Table 1. The shifts reported in Table 1 for addition of the streptavidin are referenced to the PVP-free nanostars, not the nanostars containing biotin. Thus, the total shift for biotin and protein binding is 51 nm for the ~825 nm peak. In comparison, Supporting Information Figure S3 shows the addition of both biotin and streptavidin to nanostars containing PVP. The largest shift observed was ~9 nm upon addition of both biotin and streptavidin. This is roughly 5 times less than the shift observed with capping agent-free nanostars. To determine a limit of detection and binding dissociation constant, K_d, for

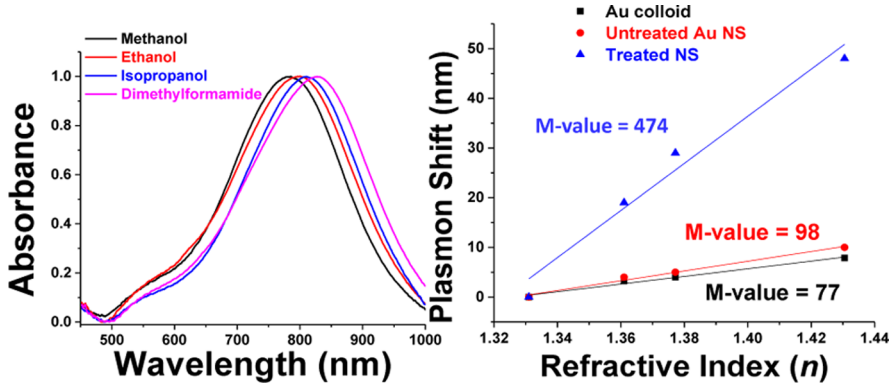

Figure 6. Sensitivity to changes in index of refraction for the plasmon absorptions of the gold nanostars treated with four 15 min treatments of sodium borohydride (60 min total). Normalized absorption spectra are shown to the left in the following solvents: Methanol, Ethanol, Isopropanol, and Dimethylformamide. Plots of the refractive index sensitivity are shown to the right. Comparison of the *m* values of gold colloids, untreated gold nanostars, and the borohydride treated gold nanostars are also shown. The untreated gold nanostars have similar *m* values to gold colloids, 98 and 77 nm/RIU respectively, whereas the borohydride treated gold nanostars exhibit a drastically improved *m* value of 474 nm/RIU.

DOI: 10.1021/acs.analchem.5b00014
Anal. Chem. 2015, 87, 3964−3972

Table 1. Observed Shifts with Standard Deviations for the Main Plasmon Absorption Band of Gold Nanostars upon PVP Removal, Biotin or Antibody Addition, and Saturating Streptavidin or PSA Addition

	LSPR Shifts, $\Delta\lambda$		
sample	without PVP (nm)	with biotin or antibody (nm)	with streptavidin or PSA (nm)
streptavidin in buffer	−43 ± 3	+19 ± 3	+51 ± 3
PSA antigen in buffer	−41 ± 3	+88 ± 3	+127 ± 3
PSA antigen in serum	−44 ± 4	+102 ± 3	+131 ± 2
PSA antigen aggregation in buffer	−41 ± 2	+88 ± 2	+214 ± 4
PSA antigen aggregation in serum	−45 ± 3	+102 ± 3	+180 ± 4

these nanostar biosensors, varying concentrations of streptavidin protein were added to an aqueous solution of PVP-free gold nanostars. As shown in Supporting Information Figure S2, the data fit well to a Langmuir isotherm in which it is assumed that only one site on the streptavidin protein is bound to the biotinylated nanostar surface. The sigmoidal fit reveals a K_d of 1×10^{-11} M, which represents the streptavidin concentration required to bind 50% of the sites. Although this dissociation constant is higher than that for streptavidin binding to biotin in solution, which is $\sim 1 \times 10^{-14}$ M, it is consistent with streptavidin binding to other nanoparticle substrates, such as the nanosphere lithography (NSL)[44] and gold nanorods.[45]

To determine the limit of detection, a control experiment was carried out in which similar concentrations of streptavidin were added to PVP-free nanostars with no biotin attached. This measurement of nonspecific binding, shown as the pink region in the binding curve in Supporting Information Figure S2, reveals a 5−6 nm shift throughout a range of streptavidin concentrations from 10^{-14} M to 10^{-8} M. This small discernible shift of ∼5 nm is evident at the lower regions of the binding curve and provides an explanation for the nonzero values before binding appears to take place. The sum of this nonspecific binding and four times the noise of the instrument, which was measured to be 0.5 nm (Supporting Information Figure S5), gives a value of 5 + 2 nm. The limit of detection was then determined by the smallest concentration required to yield a shift of 7 nm, which is 1×10^{-13} M or 0.1 pM. It is important to note that this binding curve represents a bulk average of an inhomogeneous distribution of nanostars in solution. Single nanoparticle measurements of PVP-free nanostars, which can isolate nanostars of optimal plasmonic features, would most likely reveal much lower K_d values, as well as lower limits of detection. To evaluate whether the surface of the nanostars are fully coated with streptavidin protein, a calculation of the surface coverage using the maximum LSPR shift observed was carried out (see Supporting Information). This calculation reveals a surface coverage of 5.9×10^{12} molecules/cm^2. This value is within an order of magnitude of what is reported for protein-coated NSL arrays of ∼60 nm silver nanoprisms and DNA-coated gold films.[44,46]

Next, the PVP-free nanostars were utilized in the detection of PSA. The presence of PSA protein in the blood is indicative of prostate cancer, and its detection at low concentrations is crucial for early diagnosis and survival.[47,48] To enable PSA detection, the PVP-free nanostars were coated with a MUA/octanethiol monolayer and treated with EDC, followed by PSA antibody, and finally, varying concentrations of PSA protein. Because this assembly has two layers of protein extending from the surface of the nanostars, rather than one for the biotin−streptavidin system, it was expected that PSA binding would yield larger shifts in plasmon resonance. Indeed, unprecedented large shifts of 127 nm (when referencing the PVP-free nanostars, not those with antibody) are observed and tabulated in Table 1. The large shifts observed upon PSA addition (39 nm), which is most likely ∼10 nm from the surface of the nanostars, is indicative of longer field decay lengths for the nanostars compared with colloids, as suggested by recent studies.[49,50] These sizable shifts in plasmon resonance have allowed for a binding curve and dissociation constant, K_d, to be easily obtained. The binding dissociation constant of 9×10^{-10} M is very similar to what is observed for the PSA−antibody interaction in solution. Measurements of nonspecific binding were carried out by attaching the MUA/OT ligand without the PSA antibody, followed by addition of different concentrations of PSA. The shifts in plasmon resonance, reflecting nonspecific PSA binding to the MUA/OT-capped gold nanostars, was ∼8 nm (see Supporting Information Figure S4). Similar to streptavidin binding, the limit of detection was determined as the smallest concentration giving shifts larger than the sum of nonspecific binding and 4 times the instrument noise, which is 10^{-11} M or 10 pM.

Because PSA binding in buffer yielded such large shifts in plasmon resonance, experiments investigating PSA binding in

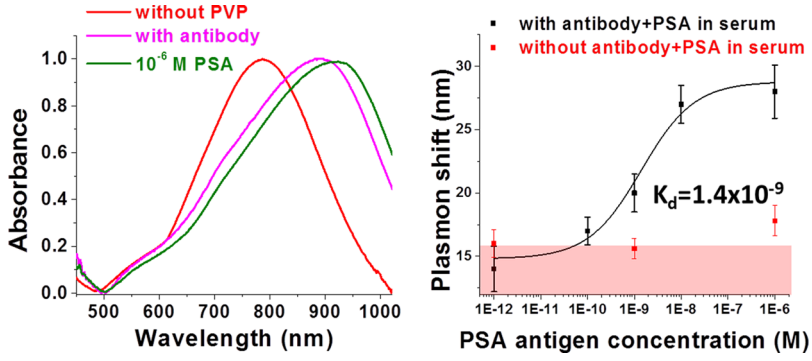

Figure 7. Biosensing with PSA protein in serum. Raw UV−vis spectra of the treated nanostars, with PSA antibody and a saturating concentration of PSA revealing shifts as large as 127 nm, left. The binding curve of PSA binding to antibody-coated nanostars, right. The pink region depicts nonspecific binding measured by mixing different concentrations of PSA with nanostars containing no antibody. Fitting the binding curve to a Lagmuir isotherm yields a K_d value of 1.4×10^{-9} M and a limit of detection of 100 pM.

DOI: 10.1021/acs.analchem.5b00014
Anal. Chem. 2015, 87, 3964−3972

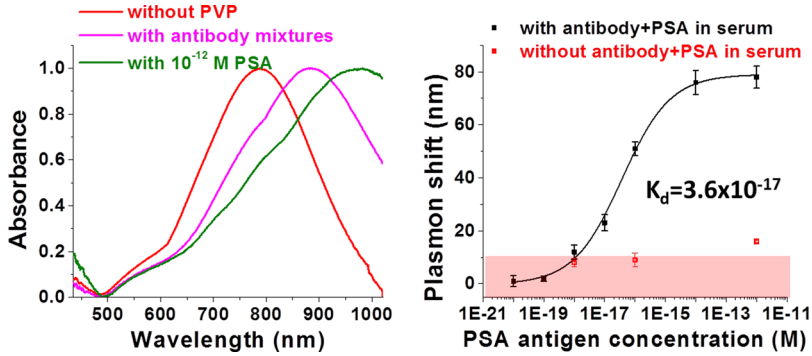

Figure 8. Biosensing using an aggregation assay with PSA protein in serum. Raw UV−vis spectra of the treated nanostars, mixture of antibody-coated nanostars without PSA, and a saturating concentration of PSA revealing shifts as large as 180 nm, left. The binding curve of PSA induced aggregation of antibody-coated nanostars, right. The pink region depicts nonspecific binding measured by mixing different concentrations of PSA with nanostars containing no antibody. Fitting the data to a Langmuir isotherm yields a K_d of 3.6 × 10−17 M and a limit of detection of 10^{-17} M.

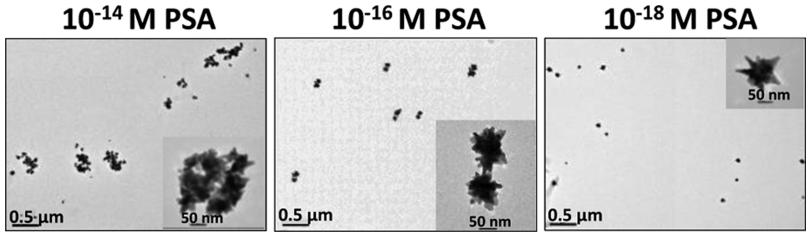

Figure 9. TEM of a mixture of gold nanostars coated with antibodies binding to different regions of the PSA protein in the presence of 10^{-14} M PSA (left), 10^{-16} M PSA (middle), and 10^{-18} M PSA (right). A systematic trend is observed, showing mostly dimers present at the intermediate PSA concentration. At higher PSA concentrations, larger aggregates are observed.

100% mouse serum were carried out. In these experiments, an antibody specifically targeting human PSA (exhibiting no affinity for mouse PSA) was utilized, followed by the addition of known concentrations of human PSA. Analogous to the experiments carried out in buffer, PVP-free nanostars were first coated in a mixture of MUA and OT, followed by the EDC coupling of PSA antibody. The coupling of the antibody was carried out in buffer, and then the assembly was transferred to serum for binding measurements. The shift observed for antibody binding to the surface of the gold nanostars in serum is ∼20 nm larger than that observed for the same nanostars in buffer, which could be due to either multilayers of antibody or nonspecific binding in serum (see Table 1). Nonspecific binding in serum was measured through addition of different concentrations of PSA to MUA-coated nanostars containing no antibody in serum. As expected, the values are roughly 2-fold higher than in buffer, and ∼14 nm shifts are observed for nonspecific binding in serum (see Figure 7). The shifts observed for PSA addition are similar to those observed in buffer, although slightly less, which may also be due to nonspecifically bound species blocking PSA binding sites on the nanostar surface. Because this value of nonspecific binding in serum is somewhat similar to the increase in shift observed for antibody addition in serum and the PSA binding shows slightly lower shifts, it is reasonable to assume that nonspecific binding is the cause of the increased shift observed for antibody binding. Finally, increasing concentrations of PSA protein were added to the antibody-coated nanostars in serum, and a binding curve was constructed (see Figure 7). The binding dissociation constant, K_d, measured from fitting the data to a Langmuir isotherm was only slightly less than that observed in buffer, 1 × 10^{-9} M. The limit of detection was determined to be 1 × 10^{-10} M or 100 pM.

To further increase the sensitivity of the nanostars to PSA binding, an aggregation assay was developed. In this aggregation assay, the gold nanostars were coated with two batches of antibodies that bind to different regions of the PSA protein. When these two batches of antibody-coated nanostars were mixed with PSA present, a "sandwich" conformation resulted, which caused nanostar aggregation. This aggregation should lead to greater shifts than the refractive-index based counterpart, due to plasmonic coupling.[49,50] This was found to be the case: the observed shifts in solution were at least 50 nm larger than those observed for the refractive-index-based measurements, giving a total shift of 214 nm when referenced to the PVP-free nanostars in buffer. Next, it was assumed that the degree of nanostar aggregation would reflect the PSA concentration; at lower PSA concentrations, less aggregation would be observed, resulting in a smaller shift, whereas at higher PSA concentrations, more aggregation would result, producing larger shifts. Indeed, the shifts were shown to be PSA-concentration-dependent, with shifts as small as 5 nm for low PSA concentrations and as large as 214 nm at saturating PSA concentrations (see Figure S6 in the Supporting Information). It should be noted that measurements were also carried out in the infrared region of the spectrum (1100−1800 nm), and no other plasmon peaks due to larger aggregates were observed.

This aggregation assay was also carried out in 100% mouse serum. Similar to the measurements carried out in buffer, the aggregation assay in serum yielded significantly larger shifts than the refractive index-based counterpart. Similar to the refractive-index-based measurements, a binding curve was constructed through addition of different concentrations of PSA in serum (see Figure 8). Although discernible shifts are observed at PSA concentrations as low as 10^{-18} M, the large

DOI: 10.1021/acs.analchem.5b00014
Anal. Chem. 2015, 87, 3964−3972

amount of nonspecific binding present in serum (11 nm) yields a limit of detection closer to 10^{-17} M.

Other sandwich assays have been carried out in which an analyte was detected through the addition of a secondary antibody attached to a gold colloid, yielding an amplification of signal and lower limit of detection.[51−54] These studies have shown increased sensitivity and limit of detection, generally by 2−3 orders of magnitude. This has been attributed to multivalent interactions in which many antibody−antigen pairs interact at the interface between the two plasmonic surfaces, thus strengthening the binding. The drastic decrease in K_d observed here (8 orders of magnitude) could be due to increased surface area at the interface between the nanostars, compared to that of a colloid, particularly when the nanostars used are substantially larger than the colloids used in previous studies. In addition, this study was carried out in a solution in which multiple nanostars were agglomerated at high PSA concentrations (see Figure 9), also resulting in increased surface area of contact.

Characterization of the aggregation process at different PSA concentrations was carried out using TEM and reveal a very systematic, controlled aggregation process (see Figure 9). Measurements show that large aggregates are observed only at higher PSA concentrations (>10^{-16} M), and low concentrations of PSA did not lead to aggregation (<10^{-18} M). Interestingly, an intermediate concentration of PSA, 10^{-16} M, yielded mainly dimer particles, which could be very useful in surface enhanced Raman spectroscopy measurements. To our knowledge, these measurements represent the first systematic aggregation of gold nanostars.

Control Experiments. Three control experiments were carried out to verify that the shifts in plasmon resonance observed were, indeed, due to specific protein binding. The first control is a measurement of nonspecific binding and is shown with the binding curves in Figures 7 and 8. This experiment involved adding the protein of interest (either streptavidin or PSA) to nanostars containing either no biotin or no PSA antibody. Although the shifts observed, particularly in serum, are sizable, they are still on the order of 10 times less than what is observed with the protein of interest present. The second control experiment, shown in Supporting Information Figure S7, involved adding a mixture of PSA and the PSA antibody to nanostars containing antibody. The idea is that the antibodies in solution would first bind to the PSA protein, making it "inactivate" toward binding the nanostar surface. Indeed, only a small shift of 1.7 nm was observed when adding this mixture to nanostars containing PSA antibody. The last control experiment, shown in Supporting Information Figure S8, involved adding high concentrations (1 mg/mL) of BSA to nanostars containing PSA antibody. This measures the nonspecific binding of other protein species that might be present in complex biological solutions, such as serum. A shift of 8 nm was observed upon addition of 1 mM BSA, which is still significantly smaller than the shifts observed upon PSA addition.

CONCLUSIONS

By removing the capping agent from gold nanostars, we have created one of the most sensitive solution-phase plasmonic biosensors. The removal of PVP is confirmed by directly measuring PVP released into solution, the blue-shifting plasmon resonances of the gold nanostars for the PVP-coated vs PVP-free samples, and SERS measurements comparing PVP-coated and PVP-free nanostars. Significantly larger refractive index sensitivity is observed for PVP-free nanostars when compared with the PVP-coated counterpart. This greatly increased sensitivity is then utilized in a series of biosensing measurements showing remarkable sensitivity in 100% serum. Last, an aggregation assay is developed to detect ultralow concentrations of PSA in serum and is shown to exhibit a limit of detection of 10^{-17} M. This aggregation assay yielded systematic changes in the aggregation state with PSA concentration and can be further utilized as a reproducible ultrasensitive SERS substrate. The capping agent-free gold nanostars, with increased LSPR sensitivity, SERS enhancement, and amenability toward functionalization, should prove extremely useful for applications ranging from single molecule spectroscopy and catalysis to in vivo biosensing, imaging, and drug delivery applications.

ASSOCIATED CONTENT

Supporting Information

Detailed information on streptavidin and PSA binding in buffer as well as results from control experiments. This material is available free of charge via the Internet at http://pubs.acs.org.

AUTHOR INFORMATION

Corresponding Author

*Phone: +1 513 556 1034. Fax: +1 513 556 9239. E-mail: saglela@uc.edu.

Notes

The authors declare no competing financial interest.

ACKNOWLEDGMENTS

This work was supported by University of Cincinnati start-up funds and a National Science Foundation funded Research Experience for Undergraduates program (NSF-REU CHE-1156449) for Carlos Matti.

REFERENCES

(1) Maier, S. A.; Kik, P. G.; Atwater, H. A.; Meltzer, S.; Harel, E.; Koel, B. E.; Requicha, A. A. G. *Nat. Mater.* **2003**, *2*, 229−232.
(2) Hutter, E.; Fendler, J. H. *Adv. Mater.* **2004**, *16*, 1685−1706.
(3) Shim, M.; Guyot-Sionnest, P. *Nature* **2000**, *407*, 981−983.
(4) Linic, S.; Christopher, P.; Xin, H. L.; Marimuthu, A. *Acc. Chem. Res.* **2013**, *46*, 1890−1899.
(5) Kang, B.; Afifi, M. M.; Austin, L. A.; El-Sayed, M. A. *ACS Nano* **2013**, *7*, 7420−7427.
(6) Sagle, L. B.; Ruvuna, L. K.; Ruemmele, J. A.; Van Duyne, R. P. *Nanomedicine* **2011**, *6*, 1447−1462.
(7) Willets, K. A.; Van Duyne, R. P. *Annu. Rev. Phys. Chem.* **2007**, *58*, 267−297.
(8) Kelly, K. L.; Coronado, E.; Zhao, L. L.; Schatz, G. C. *J. Phys. Chem. B* **2003**, *107*, 668−677.
(9) Bar-Ilan, O.; Albrecht, R. M.; Fako, V. E.; Furgeson, D. Y. *Small* **2009**, *5*, 1897−1910.
(10) Sosa, I. O.; Noguez, C.; Barrera, R. G. *J. Phys. Chem. B* **2003**, *107*, 6269−6275.
(11) Murphy, C. J.; Gole, A. M.; Stone, J. W.; Sisco, P. N.; Alkilany, A. M.; Goldsmith, E. C.; Baxter, S. C. *Acc. Chem. Res.* **2008**, *41*, 1721−1730.
(12) Huang, X. H.; El-Sayed, I. H.; Qian, W.; El-Sayed, M. A. *J. Am. Chem. Soc.* **2006**, *128*, 2115−2120.
(13) Dai, C. Y.; Zhang, A. F.; Li, L. L.; Hou, K. K.; Ding, F. S.; Li, J.; Mu, D. Y.; Song, C. S.; Liu, M.; Guo, X. W. *Chem. Mater.* **2013**, *25*, 4197−4205.
(14) Jin, R. C.; Egusa, S.; Scherer, N. F. *J. Am. Chem. Soc.* **2004**, *126*, 9900−9901.

DOI: 10.1021/acs.analchem.5b00014
Anal. Chem. 2015, 87, 3964−3972

(15) Busbee, B. D.; Obare, S. O.; Murphy, C. J. *Adv. Mater.* **2003**, *15*, 414−416.
(16) Mohanty, A.; Garg, N.; Jin, R. C. *Angew. Chem., Int. Ed.* **2010**, *49*, 4962−4966.
(17) Personick, M. L.; Langille, M. R.; Wu, J. S.; Mirkin, C. A. *J. Am. Chem. Soc.* **2013**, *135*, 3800−3803.
(18) Kumar, P. S.; Pastoriza-Santos, I.; Rodriguez-Gonzalez, B.; Garcia de Abajo, F. J.; Liz-Marzan, L. M. *Nanotechnology* **2008**, *19*, 015606.
(19) Cobley, C. M.; Au, L.; Chen, J. Y.; Xia, Y. N. *Expert Opin. Drug Delivery* **2010**, *7*, 577−587.
(20) Dam, D. H. M.; Lee, J. H.; Sisco, P. N.; Co, D. T.; Zhang, M.; Wasielewski, M. R.; Odom, T. W. *ACS Nano* **2012**, *6*, 3318−3326.
(21) Anker, J. N.; Hall, W. P.; Lyandres, O.; Shah, N. C.; Zhao, J.; Van Duyne, R. P. *Nat. Mater.* **2008**, *7*, 442−453.
(22) Nehl, C. L.; Liao, H. W.; Hafner, J. H. *Nano Lett.* **2006**, *4*, 683−688.
(23) Khoury, C. G.; Vo-Dinh, T. *J. Phys. Chem. C* **2008**, *112*, 18849−18859.
(24) Hrelescu, C.; Sau, T. K.; Rogach, A. L.; Jackel, F.; Feldmann, J. *Appl. Phys. Lett.* **2009**, *94*, 153113.
(25) Rodriguez-Lorenzo, L.; Alvarez-Puebla, R. A.; Pastoriza-Santos, I.; Mazzucco, S.; Stephan, O.; Kociak, M.; Liz-Marzan, L. M.; de Abajo, F. J. G. *J. Am. Chem. Soc.* **2009**, *131*, 4616−4618.
(26) Rodriguez-Lorenzo, L.; de la Rica, R.; Alvarez-Puebla, R. A.; Liz-Marzan, L. M.; Stevens, M. M. *Nat. Mater.* **2012**, *11*, 604−607.
(27) Dondapati, S. K.; Sau, T. K.; Hrelescu, C.; Klar, T. A.; Stefani, F. D.; Feldmann, J. *ACS Nano* **2010**, *4*, 6318−6322.
(28) Ansar, S. M.; Arneer, F. S.; Hu, W. F.; Zou, S. L.; Pittman, C. U.; Zhang, D. M. *Nano Lett.* **2013**, *13*, 1226−1229.
(29) Mayer, K. M.; Hafner, J. H. *Chem. Rev.* **2011**, *111*, 3828−3857.
(30) Enustun, B. V.; Turkevich, J. *J. Am. Chem. Soc.* **1963**, *85*, 3317−3328.
(31) Frens, G. *Nat. Phys. Sci.* **1973**, *241*, 20−22.
(32) Graf, C. D.; Vossen, L. J.; Imhof, A.; van Blaaderen, A. *Langmuir* **2003**, *19*, 6693−6700.
(33) Borodko, Y.; Habas, S. E.; Koebel, M.; Yang, P. D.; Frei, H.; Somorjai, G. A. *J. Phys. Chem. B* **2006**, *110*, 23052−23059.
(34) Tavlarakis, P.; Urban, J. J.; Snow, N. *J. Chromatogr. Sci.* **2011**, *49*, 457−462.
(35) Schlesing, H. I.; Brown, H. C.; Finholt, A. E.; Gilbreath, J. R.; Hoekstra, H. R.; Hyde, E. K. *J. Am. Chem. Soc.* **1953**, *75*, 215−219.
(36) Kojima, Y.; Suzuki, K.; Fukumoto, K.; Sasaki, M.; Yamamoto, T.; Kawai, Y.; Hayashi, H. *Int. J. Hydrogen Energy* **2002**, *27*, 1029−1034.
(37) Nehl, C. L.; Liao, H. W.; Hafner, J. H. *Nano Lett.* **2006**, *6*, 683−688.
(38) Lee, J.; Hua, B.; Park, S.; Ha, M.; Lee, Y.; Fan, Z.; Ko, H. *Nanoscale* **2014**, *6*, 616−623.
(39) Burda, C.; Chen, X. B.; Narayanan, R.; El-Sayed, M. A. *Chem. Rev.* **2005**, *105*, 1025−1102.
(40) Barbosa, S.; Agrawal, A.; Rodriguez-Lorenzo, L.; Pastoriza-Santos, I.; Alvarez-Puebla, R. A.; Kornowski, A.; Weller, H.; Liz-Marzan, L. M. *Langmuir* **2010**, *26*, 14943−14950.
(41) Rodriguez-Lorenzo, L.; Alvarez-Puebla, R. A.; de Abajo, F. J. G.; Liz-Marzan, L. M. *J. Phys. Chem. C* **2010**, *114*, 7336−7340.
(42) Shao, L.; Susha, A. S.; Cheung, L. S.; Sau, T. K.; Rogach, A. L.; Wang, J. F. *Langmuir* **2012**, *28*, 8979−8984.
(43) Chen, H. J.; Kou, X. S.; Yang, Z.; Ni, W. H.; Wang, J. F. *Langmuir* **2008**, *24*, 5233−5237.
(44) Haes, A. J.; Van Duyne, R. P. *J. Am. Chem. Soc.* **2002**, *124*, 10596−10604.
(45) Nusz, G. J.; Marinakos, S. M.; Curry, A. C.; Dahlin, A.; Hook, F.; Wax, A.; Chilkoti, A. *Anal. Chem.* **2008**, *80*, 984−989.
(46) Huang, E.; Zhou, F.; Deng, L. *Langmuir* **2000**, *16*, 3272−3280.
(47) Thompson, I. M.; Pauler, D. K.; Goodman, P. J.; Tangen, C. M.; Lucia, M. S.; Parnes, H. L.; Minasian, L. M.; Ford, L. G.; Lippman, S. M.; Crawford, E. D.; Crowley, J. J.; Coltman, C. A. *New Engl. J. Med.* **2004**, *350*, 2239−2246.
(48) Barry, M. J. *New Engl. J. Med.* **2001**, *344*, 1373−1377.
(49) Haes, A. J.; Zou, S. L.; Schatz, G. C.; Van Duyne, R. P. *J. Phys. Chem. B* **2004**, *108*, 109−116.
(50) Lyon, L. A.; Musick, M. D.; Natan, M. *Anal. Chem.* **1998**, *70*, 5177−5183.
(51) Kim, H. M.; Jin, S. M.; Lee, S. K.; Kim, M. G.; Shin, Y. B. *Sensors* **2009**, *9*, 2334−2344.
(52) Buckle, P. E.; Davies, R. J.; Kinning, T.; Yeung, D.; Edwards, P. R.; Pollard-Knight, D. *Biosens. Bioelectron.* **1993**, *8*, 355−363.
(53) Lyon, L. A.; Musick, M. D.; Natan, M. J. *Anal. Chem.* **1998**, *70*, 5177−5183.
(54) Hall, W. P.; Ngatia, S. N.; Van Duyne, R. P. *J. Phys. Chem. C* **2011**, *115*, 1410−1414.

DOI: 10.1021/acs.analchem.5b00014
Anal. Chem. 2015, 87, 3964−3972